Preprints are preliminary reports that have not undergone peer review. They should not be considered conclusive, used to inform clinical practice, or referenced by the media as validated information.

Consequences of Quantum Noise Control for the Relaxation Resonance Frequency and Phase Noise in Heterogeneous Silicon/III-V Lasers

Dongwan Kim (dongwan.kim@caltech.edu)
California Institute of Technology
Mark Harfouche
California Institute of Technology
Huolei Wang
California Institute of Technology
Christos T. Santis
California Institute of Technology
Yaakov Vilenchik
California Institute of Technology
Naresh Satyan
Telaris Inc
George Rakuljic
Telaris Inc
Amnon Yariv
California Institute of Technology

Research Article

Keywords: semiconductor laser, Schawlow-Townes linewidth, resonance frequency, laser footprint

Posted Date: July 12th, 2021

DOI: https://doi.org/10.21203/rs.3.rs-686549/v1

License: This work is licensed under a Creative Commons Attribution 4.0 International License.
Read Full License

Version of Record: A version of this preprint was published at Scientific Reports on January 10th, 2022. See the published version at https://doi.org/10.1038/s41598-021-03314-8.

Consequences of quantum noise control for the relaxation resonance frequency and phase noise in heterogeneous Silicon/III-V lasers

Dongwan Kim[1,*,+], Mark Harfouche[2,+], Huolei Wang[1,†], Christos T. Santis[1], Yaakov Vilenchik[1], Naresh Satyan[3], George Rakuljic[3], and Amnon Yariv[1,2]

[1]Department of Applied Physics and Materials Science, California Institute of Technology, Pasadena, California 91125, USA
[2]Department of Electrical Engineering, California Institute of Technology, Pasadena, California 91125, USA
[3]Telaris Inc., Santa Monica, California 90403, USA
[*]Corresponding author: dongwan.kim@caltech.edu
[+]these authors contributed equally to this work

ABSTRACT

We have recently introduced a new semiconductor laser design which is based on an extreme, 99%, reduction of the laser mode absorption losses. This was achieved by a laser mode design which confines the great majority of the modal energy (> 99%) in a low-loss Silicon guiding layer rather than in highly-doped, thus lossy, III-V p^+ and n^+ layers, which is the case with traditional III-V lasers. The resulting reduced electron-field interaction leads directly to a commensurate reduction of the spontaneous emission rate by the excited conduction band electrons into the laser mode and thus to a reduction of the frequency noise spectral density of the laser field often characterized by the Schawlow-Townes linewidth. In this paper, we demonstrate theoretically and present experimental evidence of yet another major beneficial consequence of the new laser design: a near total elimination of the contribution of amplitude-phase coupling (the Henry α parameter) to the frequency noise at "high" frequencies. This is due to an order of magnitude lowering of the relaxation resonance frequency of the laser. The practical elimination of this coupling enables yet another order of magnitude reduction of the frequency noise at high frequencies, resulting in a quantum-limited frequency noise spectral density of 130 $\mathrm{Hz}^2/\mathrm{Hz}$ (linewidth of 0.4 kHz) for frequencies beyond 680 MHz. This development is of key importance in the drive to semiconductor lasers with higher coherence, particularly in the context of integrated photonics with a small laser footprint.

Introduction

The semiconductor laser (SCL) has become and, very likely, will continue to be, in the foreseeable future, the linchpin of optoelectronics[1–5]. A few major obstacles, however, remain before the promise of CMOS-like Photonic Integrated Circuits (PICs) can be realized. Chief among these problems is: low-coherence, the dependence on external isolators to reduce optical feedback, and the coherence-reducing amplitude-phase coupling. Recently[6,7], we have shown how the "removal" by modal design of optical energy from the lossy III-V material to low-loss material, Silicon in our example, reduces the frequency noise due to spontaneous emission and improves the field coherence by some three orders of magnitude, with the improvement being limited by the residual losses of the Silicon (or, more precisely, by the Q-factor of the laser mode). An unexpected bonus of the high-Q laser was its improved, 20-25 dB in our laboratory-fabricated lasers, insensitivity to optical feedback [8,9]. This improvement is again limited by the achievable intrinsic Q of the laser mode.

In this paper, we provide theoretical arguments and experimental evidence that the reduced interaction of the excited electrons in the SCL with the quantum-mandated zero-point field of the laser mode in our laser design leads, additionally, to a practical elimination of the amplitude-phase coupling at frequencies above that the relaxation resonance[10]. The order, or orders, of magnitude improvements in these three key metrics of the SCL are archived while maintaining its small size and the CMOS-fabrication compatibility. Taken together, they pave the way to a new generation of SCLs with intrinsic ultra-high-Q values as the main enablers of high-coherence photonic integrated circuits[11].

In this paper, we take an ab-initio look at the relationships between some of the key attributes of the semiconductor laser; specifically, the current modulation response, phase-amplitude coupling, relaxation resonance, and the frequency noise (or phase noise). In the experimental section, we describe how the theoretical results are applied to the design of semiconductor lasers and present the measured relevant characteristics of these lasers. We use the heterogeneous Silicon/III-V laser as a proof-of-concept platform.

Semiconductor laser theory

Relaxation resonance frequency and the Schawlow-Townes linewidth

A convenient starting point in the analysis of the phase noise of a semiconductor laser is to consider the problem of the current modulation response. We start with the set of coupled equations for the number of photons n_l in the lasing mode of the laser resonator and for the number of inverted electrons n_e in the active regions[12],

$$\frac{dn_e}{dt} = \eta_i \frac{I}{q} - \frac{n_e}{\tau_e} - W_{sp}^{(l)}(n_e - n_{tr})n_l, \tag{1}$$

$$\frac{dn_l}{dt} = \left[W_{sp}^{(l)}(n_e - n_{tr}) - \frac{1}{\tau_p}\right] n_l, \tag{2}$$

where η_i is an injection efficiency of the electrons into the active region, I is the injected current to the laser, τ_e is the electron recombination time, n_{tr} is the number of electrons at transparency, and τ_p is the photon cavity lifetime for the lasing mode.

Here, the photon cavity lifetime accounts for the intrinsic losses in the cavity τ_i due to scattering and absorption, and losses due to useful output coupling τ_{ext}. $W_{sp}^{(l)}$ is the spontaneous emission rate into the lasing mode (l), a material-dependent constant. We choose the total number of photons and the total number of excited electrons as our main variables rather than their densities since according to the quantum mechanics that describe the interaction between photons and electrons, a single electronic transition results in the emission or the absorption of one photon.

A key result of these equations is the intensity modulation (IM) response, defined as the ratio of the amplitude of the total emitted power modulation ΔP_{out} at a frequency f to the amplitude of the driving current ΔI at f, and is given by:

$$H(f) = \frac{\Delta P_{out}(f)}{\Delta I(f)} = \frac{\eta_d h\nu/q}{1-(f/f_R)^2 + i(f/f_R)(2\pi f_R \tau_p + 1/(2\pi f_R \tau_e))}, \tag{3}$$

$$f_R = \frac{1}{2\pi}\sqrt{\eta_i \frac{W_{sp}^{(l)}(I - I_{th})}{q}}. \tag{4}$$

This transfer function $H(f)$ is that of a second-order low-pass filter response whose magnitude is constant at low frequencies. At higher frequencies, above that of the relaxation resonance frequency f_R, $H(f)$ drops by 40 dB per octave. It is consequently used as a measure of the upper limit to the response of the laser intensity to current modulation. $H(f)$, as will be shown below, also plays a key role in the laser temporal coherence. It can be seen from Equation 4 that f_R is proportional to the square root of the spontaneous emission rate determined by the strength of the interaction between the electrons and the lasing mode. Following an ab-initio analysis of the quantum interaction between the excited electron and the lasing mode, we find that the spontaneous and stimulated transition rates of an electron from an excited state in the conduction band to an unoccupied state in the valence band, due to the interaction with the lasing mode (l) in Equation 1 and 2, are given by [6,7,13]:

$$W_{sp}^{(l)} = \frac{2\pi^2\mu^2\nu_l g_a(\nu_l)}{h\varepsilon(\bar{r}_a)}\left|\bar{E}_l(\bar{r}_a)\right|^2, \tag{5}$$

$$W_{st}^{(l)} = n_l W_{sp}^{(l)}, \tag{6}$$

where μ is the dipole transition matrix element, $g_a(\nu_l)$ is the value of the normalized lineshape function of the transition at the lasing frequency ν_l (both known quantities for our purposes). $\varepsilon(\bar{r}_a)$ is the permittivity of the bulk material at the location of the emitter. $\left|\bar{E}_l(\bar{r}_a)\right|^2$ is the normalized intensity of the laser mode at the location of the emitter $\bar{r}_a$ (i.e., electron). Integrated over the volume of the quantum wells, $\left|\bar{E}_l(r_a)\right|^2$ yields the confinement factor (Γ) of the electric field in the active region (i.e., $\left|\bar{E}_l(r_a)\right|^2 \propto \Gamma_{QW}$)[14]. Combined with Equation 4, we find that

$$f_R \propto \left|\bar{E}_l(\bar{r}_a)\right|\sqrt{I - I_{th}}. \tag{7}$$

This result highlights one key parameter in the control of the relaxation resonance frequency f_R: *the magnitude of the electric field at the location of the emitter*. Similarly, we obtain the damping coefficient γ of the second-order response,

$$\gamma = \frac{1}{2}\left(2\pi f_R \tau_p + \frac{1}{2\pi f_R \tau_e}\right) \propto \frac{1}{\left|\bar{E}_l(\bar{r}_a)\right|}. \tag{8}$$

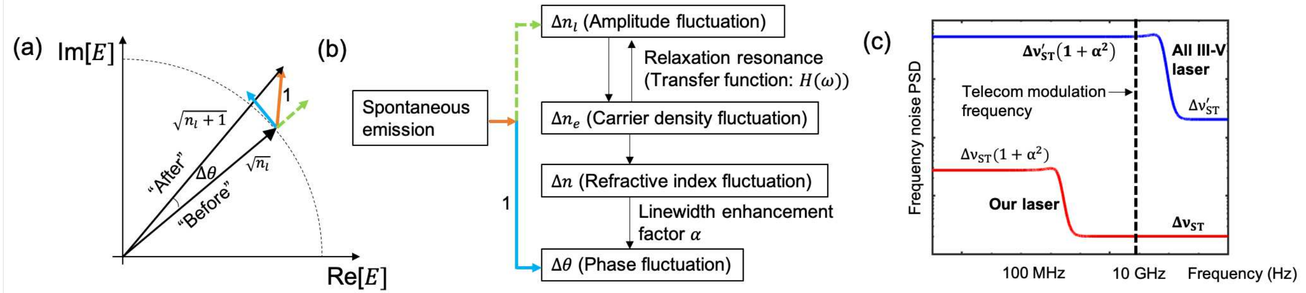

Figure 1. (a) The phasor model for the laser field phase, showing the electric field before and after a single spontaneous emission event (orange arrow). The projection of the spontaneous emission event onto the phase and intensity quadrature is shown in the blue solid and green dotted line respectively. (b) Phase noise due to spontaneous emission including both the direct spontaneous emission phase noise and the additional phase noise via the amplitude-phase coupling. (c) A cartoon illustrating the expected frequency noise power spectral density of the high-coherence Silicon/III-V laser and the conventional III-V laser.

As a consequence, as we decrease $\left|\overline{E}_l\left(\overline{r}_{\mathrm{a}}\right)\right|$, we find that the damping coefficient of the response increases giving these lasers an over-damped response to spontaneous emission generated in the gain region ensuring that the intensity noise is monotonically decreasing without the presence of any peak near the relaxation resonance frequency, which is observed in the case of an under-damped response.

To understand how the relaxation resonance frequency affects the phase noise, we now look into the phase noise caused by the spontaneous emission events. At frequencies high enough where thermal noise can be ignored in semiconductor lasers, the spontaneous emissions become the dominant source of noise that perturbs the lasing field circulating in the cavity[10]. Furthermore, while thermal and electrical noise sources can be mitigated by improving the thermal and electronic design of the driving circuit, the origin of spontaneous emission is quantum mechanical and cannot be avoided thus determining the ultimate noise floor of the laser. These quantum perturbations can be analyzed as two distinct noise sources, one coupled to the amplitude quadrature, and the other coupled to the phase quadrature, as shown in Figure 1 (a). The first component is perpendicular to the phasor of the electric field and couples directly to the phase of the optical field (blue solid line in Figure 1 (a)). The second component, parallel to the phasor of the field, alters the intensity of the lasing field (green dotted line in Figure 1 (a)). To compensate for the change in intensity, the gain-providing carriers fluctuate in response to these amplitude changes in an attempt to restore the steady-state output intensity of the laser. In semiconductor lasers, changes in the carrier concentration induce a corresponding proportional change in the refractive index leading to additional frequency noise through Kramers-Kroning relations[12]. Thus, fluctuations in the total number of carriers manifest themselves as additional phase fluctuations through a process known as amplitude-phase coupling depicted in Figure 1 (b).

Mathematically, the results of Equation 2 are such that the change in carrier number due to quantum fluctuations in the cavity exhibits the same second-order response cut off at a relaxation resonance f_R. As a consequence, the power spectral density (PSD) of the additional frequency noise due to the amplitude-phase coupling exhibits the same frequency dependence as the intensity modulation response $H(f)$ of a directly modulated laser[15,16]. Therefore, in the quantum-limit, the frequency noise PSD (single-sided) of a semiconductor laser can be expressed as the sum of two terms[13],

$$S_{\Delta\nu}(f) = \frac{n_{2\mathrm{th}} W_{\mathrm{sp}}^{(l)}}{4\pi^2 n_l}\left(1+\alpha^2\left|H(f)\right|^2\right), \tag{9}$$

where $n_{2\mathrm{th}}$ is the total number of electrons in the conduction band at threshold. The first term $\frac{n_{2\mathrm{th}} W_{\mathrm{sp}}^{(l)}}{4\pi^2 n_l}$ is often referred to as the Schawlow-Townes linewidth, representing the intrinsic, quantum-limited, ultimate noise floor including only the direct spontaneous emission phase noise. The additional phase noise due to the amplitude-phase coupling gives rise to linewidth enhancement factor α, which ranges between 2 and 6 for the case of broadly-used quantum-well (QW) semiconductor lasers[14,17,18].

As such, for lasers with a relaxation resonance frequency $f_R \approx 10$ GHz, the amplitude-phase coupling constitutes the majority of the spontaneous-emission-induced frequency noise for semiconductor lasers in the frequency bands of interest for high-speed sensing and communication with sampling rates in the few GHz, as shown in Figure 1 (c). However, if one can design lasers with a relaxation resonance frequency positioned at the range of hundreds of MHz, then the total frequency noise of the lasers will drop by a factor of $(1+\alpha^2)$ at frequencies of GHz leaving only the white noise floor generated by the direct spontaneous emission events.

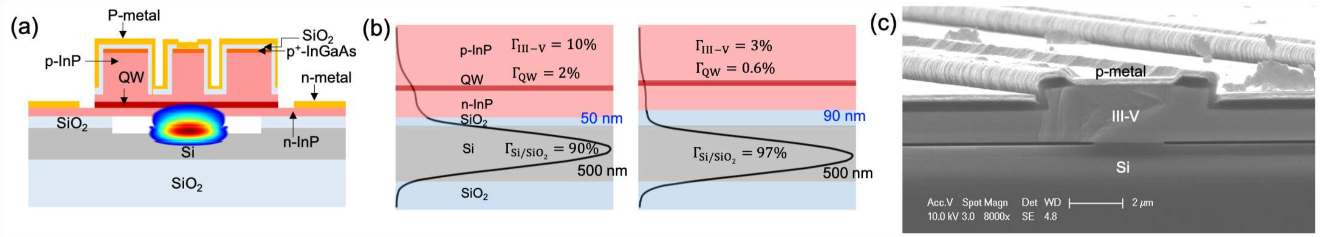

Figure 2. (a) Cartoon cross-sectional view of the laser device structure. (b) Transverse optical mode profile in the lasers with the 50 nm and 90 nm SiO_2 quantum noise control layer together with the confinement factor in each layer. (c) SEM image of the cross-section of the fabricated laser.

In the rest of the paper, we will refer to the "enhanced linewidth" as the value that includes the carrier-induced frequency noise ($\Delta\nu_{\text{enhanced}} = \pi S_{\Delta\nu}(f < f_{\text{R}}) = \frac{n_{2\text{th}} W_{\text{sp}}^{(l)}}{4\pi n_l}(1+\alpha^2) = \Delta\nu_{\text{ST}}(1+\alpha^2)$) and to the "Schawlow-Townes linewidth" as the value proportional to the direct contribution of spontaneous emission to phase noise ($\Delta\nu_{\text{ST}} = \pi S_{\Delta\nu}(f > f_{\text{R}}) = \frac{n_{2\text{th}} W_{\text{sp}}^{(l)}}{4\pi n_l}$)[19].

Frequency noise above the relaxation resonance frequency of the high-coherence Silicon/III-V lasers

In our recently reported quantum noise controlled Silicon/III-V lasers[6,7], we harnessed the Purcell effect to decrease the spontaneous emission rate into the lasing mode. This was achieved by utilizing a SiO_2 layer between the Silicon and III-V ranging from 50 nm to 150 nm, which we call the quantum noise control layer (QNCL), to engineer the optical mode's spatial distribution with respect to the emitter ($\left|\overline{E}_l\left(\overline{r}_{\text{a}}\right)\right|$). The geometry of the cross-section and the transverse optical mode profile for the case of the 50 nm and 90 nm SiO_2 QNCL lasers are shown in Figure 2 (b). Using this strategy, we have shown that Silicon/III-V lasers employing a monolithically integrated high-Q resonator can have linewidths as small as a few kHz without sacrificing the parameters such as the threshold current (due to the constant $n_{2\text{th}}$) and the optical output power. The strategy is effective as long as the laser mode losses are dominated by absorption in the III-V or, equivalently, as long as the overall Q of the laser mode is dominated by III-V losses, which we estimate occurs when the thickness of the SiO_2 layer is approximately 150 nm. Further reduction in the electric field strength at the quantum-well layer results in the increase in the threshold carrier density to maintain the gain that matches the no-longer-decreasing modal loss, increasing the threshold current.

To investigate the effect of the reduced electric field strength at the location of the quantum-wells on the relaxation resonance of the lasers, we revisit Equation 7. Due to the dependence of the relaxation resonance frequency on the square root of the intensity of the electric field at the quantum-well emitter, every two orders of magnitude reduction in the field strength at the quantum-well will result in the reduction of one order of magnitude in the relaxation resonance frequency. In our demonstration, we've reduced $\Gamma_{\text{III-V}} = 100\%$ for conventional all III-V laser to $\Gamma_{\text{III-V}} = 1\%$ ($\Gamma_{\text{QW}} = 0.2\%$) for the case of the 150 nm QNCL laser resulting nearly in a full order of magnitude reduction in the relaxation resonance frequency of the laser from a few GHz to hundreds of MHz[20,21] .

Figure 1 (c) illustrates that at frequencies of a few GHz, conventional III-V lasers still exhibit "enhanced frequency noise" including both the direct spontaneous emission phase noise and the amplitude-phase-coupling-induced frequency noise. In contrast, at a few GHz, our high-coherence Silicon/III-V lasers eliminate the additional frequency noise via amplitude-phase coupling by positioning a relaxation resonance frequency at a frequency of a few hundreds of MHz, yielding lasers that possess the intrinsic, quantum-limited Schawlow-Townes noise floor.

Results and discussion

Laser design and fabrication

The high-coherence Silicon/III-V laser is based on a Silicon waveguide to which a III-V epitaxially grown stack is bonded separated by a thin SiO_2 layer (Figure 2 (a)). The oxide layer is obtained by thinning a thermally grown SiO_2 layer, originally 400 nm thick, on the top of the silicon-on-insulator (SOI) waveguide using a buffer HF wet etch. The high-Q Silicon resonator is defined by etching a 60 nm rib on a 500 nm thick Silicon device layer creating a 2.5 µm wide waveguide. In the same fabrication steps, a 1-D grating is etched in the waveguide to define the optical cavity by etching holes 60 nm wide in the direction of propagation and of varying width.

The width of the gratings in the defection section varies between 200 nm and 300 nm in the transverse direction along the length of the resonator such that the 240 µm-long defect has a photonic well that contains a single high-Q mode[6]. The intrinsic Q-factor of the fabricated Silicon resonator is measured to be as high as 10^6. End reflections are provided by two mirror regions,

on either side of the defect section, of 300 μm and 400 μm long for the 50 nm and 90 nm QNCL lasers, respectively. The mirror length of the 90 nm QNCL laser is chosen to be larger than that of the 50 nm QNCL laser to increase the loaded Q-factor of the 90 nm QNCL proportionally to the expected increase in the intrinsic Q-factor. The period of the grating determines the lasing wavelength, and in our case is chosen to be 240.0 nm and 237.5 nm for the 50 nm and 90 nm QNCL lasers, respectively. The unpatterned InP is directly bonded on the pattered SOI resonators and incorporates five InGaAsP quantum-wells. Subsequently, the mesa structure and the metal contacts are patterned on the III-V wafer[22]. Figure 2 (c) shows the SEM image of the fabricated laser.

The mode has an estimated intrinsic Q-factor equal to the weighted harmonic mean of the Q-factors of the Silicon and III-V waveguides. Through finite element simulations, we estimate the confinement factor in the III-V of the 50 nm and 90 nm QNCL lasers to be 10% and 3% (Figure 2 (b)), respectively, yielding a Q-factor of approximately 1×10^5 and 2.5×10^5.

Measurements

The light-pump current (LI) and the current vs. voltage (IV) characteristics of the fabricated 50 nm and 90 nm QNCL lasers are shown in Figure 3 (a). The 50 nm and 90 nm laser obtain continuous-wave laser operation with threshold currents of 50 mA and 80 mA, respectively, and single-facet output powers more than 2 mW at 20°C. Figure 3 (b) presents the optical spectrum of the 50 nm and 90 nm lasers obtaining a single-mode operation with side-mode suppression ratios greater than 45 dB at the lasing wavelength of 1577 nm and 1556 nm, respectively.

The intensity modulation (IM) response $H(f)$ of the lasers is measured using a network analyzer (HP 8722C) and a high-speed photodetector (Optilab BPR-20-M). The IM index m, defined as $\Delta P/P_0$ per 1 mA where ΔP is the change in the optical power and P_0 is the average received optical power, is shown in Figure 4 (a) for the 50 nm QNCL laser at bias currents of 70, 90, and 130 mA. As expected, the IM response exhibits a second-order low-pass filter behavior with flat response for frequencies up to the relaxation resonance frequencies, and 40 dB/decade drop-off thereafter. Fitting the measured response to the second-order low-pass filter response in Equation 3 yields a relaxation resonance frequencies f_{R} of 380, 650, and 900 MHz at bias currents of 70, 90, and 130 mA, respectively. The relaxation resonance frequencies of the 90 nm QNCL laser, extracted from the data presented in Figure 4 (b), are measured to be 320, 540, and 610 MHz at bias currents of 100, 140, and 170 mA, respectively. These low relaxation resonance frequencies at hundreds of MHz clearly stand in contrast to those of conventional III-V lasers of a few GHz. The linear dependence of the relaxation resonance frequencies of the 50 nm and 90 nm QNCL lasers on $\sqrt{I - I_{\mathrm{th}}}$, described in Equation (7) is shown in Figure 4 (c). The reduction in the relaxation resonance frequencies f_{R} is observed with the increasing QNCL thickness, which is attributed to the reduced electric field strength $\left|\overline{E}_l\left(\overline{r}_{\mathrm{a}}\right)\right|$ at the location of the quantum-wells (i.e., reduced Γ_{QW}). It can also be observed that the relaxation resonance peak is less apparent on the 90nm QNCL laser compared to that of the 50 nm QNCL, due to the increased damping in the 90nm QNCL as predicted in Equation 8.

For the fabricated lasers, we found that the 50 nm QNCL laser, which has a lasing wavelength of 1577 nm, shows a linewidth enhancement factor of 5.8, whereas the 90 nm laser lasing at the wavelength of 1556 nm has a linewidth enhancement factor of 3. The details of the measurements follow the measurement setup and analysis of [14,23,24] and are discussed in the Supplementary Material.

To finally characterize the linewidth of the lasers, we measure the frequency noise PSD using an RF spectrum analyzer after mixing the laser light with the time-delayed version of itself at the output of the 1.575 GHz MZI. A low frequency (100 Hz)

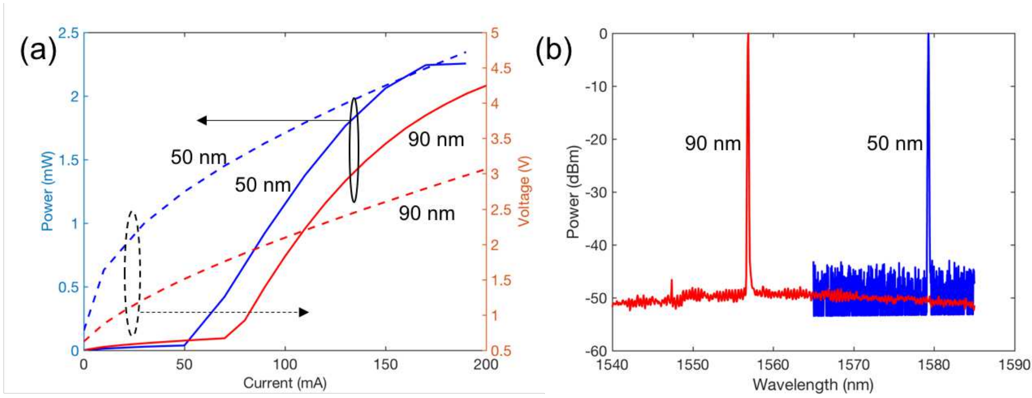

Figure 3. (a) The light vs. pump current (LI) and current vs. voltage (IV) characteristics of the 50 nm and 90 nm QNCL lasers at 20°C. (b) The optical spectrum of the lasers at 20°C, showing a single-mode operation with a side-mode suppression ratio larger than 45 dB.

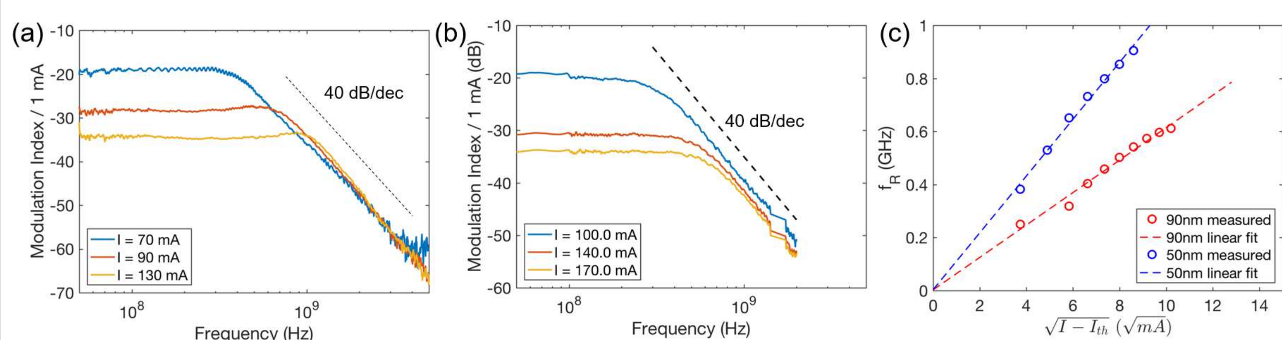

Figure 4. (a) The intensity modulation response of the 50 nm QNCL laser at different bias currents. (b) The intensity modulation response of the 90 nm QNCL laser at different bias currents. (c) Relaxation resonance frequencies of the 50 nm and 90 nm QNCL lasers as a function of $\sqrt{I-I_{\mathrm{th}}}$.

feedback loop uses a piezo fiber stretcher to keep the quadrature point of the MZI locked to the wavelength of the laser for the duration of the measurement. The measured PSD of the photocurrent fluctuation is converted to the frequency noise PSD of the laser[6].

The frequency noise PSD of the 50 nm QNCL laser ($I_{\mathrm{th}} = 50$ mA, $\lambda_0 = 1577$ nm) is shown in Figure 5 (a). The steep $1/f$ noise is observed in the low frequency region up to 10 MHz. The enhanced linewidth can be estimated when the spectrum reaches a flat white frequency noise floor between frequencies of 10 and 100 MHz, where thermal noise is heavily suppressed. In this range, the PSD ($S_{\Delta\nu}$) takes a value of 1.9×10^4 Hz^2/Hz for a bias current of 80 mA corresponding to an enhanced linewidth of 60 kHz. When the current is increased to 130 mA, the frequency noise drops to 8.9×10^3 Hz^2/Hz, corresponding to an enhanced linewidth of 28 kHz.

To characterize the Schawlow-Townes linewidth observable at frequencies above the relaxation resonance frequency f_{R}, a direct measurement of the spontaneous emission white noise floor is desirable. However, the finite output power of the lasers in this proof-of-concept demonstration made their frequency noise approach the shot-noise level at approximately 1 GHz just above the relaxation resonance frequency. As a consequence, it was not possible to measure the frequency noise much above the relaxation resonance frequency. However, we are able to observe the early effects of the low relaxation resonance frequency and its peak in the frequency range between 100 MHz and 1 GHz, which shows excellent agreement with the intensity modulation response measured in Figure 4 (a). Using Equation 9, we can extract an estimate of the Schawlow-Townes linewidth at frequencies above f_{R} by combining the measured PSD $\Delta\nu_{\mathrm{enhanced}} = \Delta\nu_{\mathrm{ST}}(1+\alpha^2)$ of the lasers below f_{R}, measurements of the modulation response $H(f)$ and linewidth enhancement factor $\alpha \approx 5.8$. We can see that the frequency noise estimate (the dashed line in Figure 5 (a)) extrapolated based on $\Delta\nu_{\mathrm{enhanced}}$, $H(f)$, α and the measured curves at both currents are in

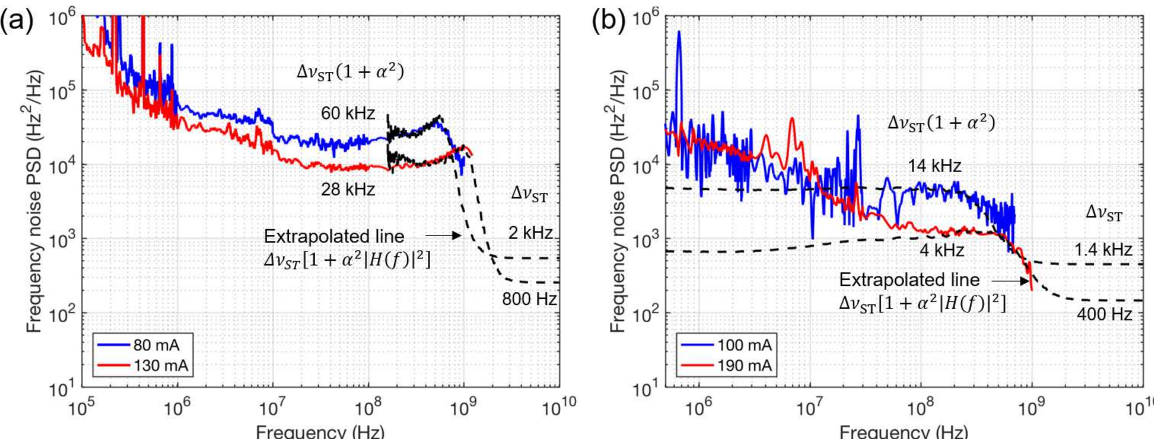

Figure 5. The frequency noise power spectral density of the lasers. The expected frequency noise at frequencies further into the GHz range is extrapolated in black dotted line using Equation 9. (a) The 50 nm QNCL laser (I_{th} = 50 mA, λ_0 = 1577 nm, α = 5.8). (b) The 90 nm QNCL laser (I_{th} = 80 mA, λ_0 = 1556 nm, α = 3.0).

good agreement up to 1 GHz. Therefore, from the extrapolated estimate, we predict that the frequency noise above f_R at a bias current of 80 mA is 540 Hz^2/Hz, yielding a Schawlow-Townes linewidth of 1.7 kHz. For the bias current of 130 mA, the frequency noise above f_R is estimated to be 250 Hz^2/Hz, corresponding to Schawlow-Townes linewidth of 0.8 kHz, achieving yet another order of magnitude decrease in the frequency noise.

The early effects of the low relaxation resonance frequency of the 90 nm QNCL laser ($I_{th} = 80$ mA, $\lambda_0 = 1556$ nm) are also observable in Figure 5 (b) where it can be seen that the frequency noise power spectral density decreases near the relaxation resonance frequency– 360 MHz and 680 MHz, as measured in the IM response, for pump currents of 100 mA and 190 mA respectively. The frequency noise estimate for the 90 nm laser is extrapolated using $\Delta\nu_{\text{enhanced}}$, $H(f)$, α of this laser and is shown in the dashed line in Figure 5 (b). The measured and the extrapolated lines show good agreement with each other up to approximately 1 GHz. Hence, we measure a frequency noise floor above f_R to be 450 Hz^2/Hz at a bias current of 100 mA, yielding a Schawlow-Townes linewidth of 1.4 kHz. At a bias current of 190 mA, the frequency noise above f_R is expected to be 130 Hz^2/Hz, achieving the Schawlow-Townes linewidth of 0.4 kHz.

Discussion

In this paper, we showed that the strategy of quantum noise control, i.e., control of the spontaneous emission rate, can decrease the relaxation resonance frequency f_R of semiconductor lasers to a few hundred MHz, resulting in the suppression of the phase noise induced by the amplitude-phase coupling and reduction in the frequency noise PSD by an additional order of magnitude. Hence, we theoretically and experimentally demonstrated that in order to decrease the frequency noise of semiconductor lasers, all three "knobs" in Equation 9, the spontaneous emission rate $W_{sp}^{(l)}$, the number of the stored photons n_l, and the transfer function of the modulation response $H(f)$ can be controlled and optimized by the low loss modal design which stores the great majority of the optical modal energy in a low-loss material rather than in the active, high-loss material.

In this work, the concept of reducing the laser phase noise by decreasing the modal loss is realized through modal engineering in the transverse direction of the waveguide. The concept of increasing the Q-factor of the laser cavity through the modal engineering is also possible in the longitudinal direction through the use of tapers to transition the optical mode between the III-V and passive low-loss waveguide, as the wave travels along the length of the resonator[25,26]. In these architectures, the confinement factor in the active region scales as the ratio of the length of the active region to the effective length of the cavity. This means that reducing the relaxation resonance frequency by an order of magnitude would require the size of the external cavity laser to scale by two orders of magnitude. However, in the lasers described here, small changes in the thickness of the SiO_2 layer on the order of tens of nanometers can change the confinement factor by a factor of 100 and can alter the relaxation resonance frequency of the laser by an order of magnitude. The transverse modal control allows us to achieve the same effect with very little compromise in footprint. Furthermore, keeping a small footprint for the laser helps ensure mode-hop free operation even as the injection current is changed.

It is notable that the magnitude of the linewidth enhancement factor α is an intrinsic property of the *gain medium*, regardless of the structure of the optical mode in the laser. Therefore, for a given material, one cannot eliminate the presence of the linewidth enhancement factor and its effect on the phase noise. Other methods used to suppress the linewidth enhancement factor include the use of quantum-dots (QDs) as the gain medium. Quantum-dots do not exhibit a linewidth enhancement factor, due to their delta function-like density of states[27,28]. However, quantum-dots still remain difficult to grow for certain materials and often exhibit lower material gain than their quantum-well counterparts. The demonstration of the suppression of the linewidth enhancement factors at a relatively low frequency in our lasers means that using this approach, lasers can obtain an effective linewidth enhancement factor of 0 in the GHz range without utilizing quantum dots as the gain providing material.

Of further importance is the dependence of the linewidth enhancement factor on the operating wavelength of the laser. As discussed in[23,24] and in agreement with our measurements of α for lasers of different operating wavelengths, lasers that operate further from the differential gain peak experience a larger linewidth enhancement factor. Lasers designed with the same gain medium operating at different wavelengths will consequently have different noise characteristics, owing to differences in the linewidth enhancement factor. This is of special importance for tunable laser designs or dense laser arrays[29]. By having low relaxation resonance frequencies, the influence of the linewidth enhancement factor can be suppressed ensuring that lasers operating at different wavelengths will have nearly identical spectral characteristics at a few GHz range.

Conclusion

We have demonstrated theoretically and experimentally that our low-loss laser modal design leads, in addition to orders of magnitude reduction of phase noise and to isolator-free operation, to relaxation resonance frequencies as low as a few hundreds of MHz in heterogeneously integrated Silicon/III-V lasers. These low relaxation resonance frequencies enable the lasers to achieve the quantum-limited Schawlow-Townes linewidth, as low as 0.4 kHz, by effectively reducing to insignificance the amplitude-phase coupling (characterized by the Henry α parameter). As new fabrication techniques continue to be refined and

new optical materials emerge, this optical modal engineering strategy can be useful for creating compact, even lower noise lasers that do not suffer from additional phase noise due to amplitude-phase coupling at a variety of operating wavelengths.

References

1. Nazarova, T., Lisdat, C., Riehle, F. & Sterr, U. Low-frequency-noise diode laser for atom interferometry. *J. Opt. Soc. Am. B* **25**, 1632–1638, DOI: 10.1364/JOSAB.25.001632 (2008).

2. Alnis, J., Matveev, A., Kolachevsky, N., Udem, T. & Hänsch, T. W. Subhertz linewidth diode lasers by stabilization to vibrationally and thermally compensated ultralow-expansion glass fabry-pérot cavities. *Phys. Rev. A* **77**, 053809, DOI: 10.1103/PhysRevA.77.053809 (2008).

3. Margolis, H. S. *et al.* Hertz-level measurement of the optical clock frequency in a single 88sr+ ion. *Science* **306**, 1355–1358, DOI: 10.1126/science.1105497 (2004). https://science.sciencemag.org/content/306/5700/1355.full.pdf.

4. Evans, P. *et al.* 1.12 tb/s superchannel coherent pm-qpsk inp transmitter photonic integrated circuit (pic). *Opt. Express* **19**, B154–B158, DOI: 10.1364/OE.19.00B154 (2011).

5. Corzine, S. W. *et al.* Large-scale inp transmitter pics for pm-dqpsk fiber transmission systems. *IEEE Photonics Technol. Lett.* **22**, 1015–1017, DOI: 10.1109/LPT.2010.2048894 (2010).

6. Santis, C. T., Steger, S. T., Vilenchik, Y., Vasilyev, A. & Yariv, A. High-coherence semiconductor lasers based on integral high-Q resonators in hybrid Si/III-V platforms. *Proc. Natl. Acad. Sci.* **111**, 2879–2884, DOI: 10.1073/pnas.1400184111 (2014). http://www.pnas.org/content/111/8/2879.full.pdf.

7. Santis, C. T., Vilenchik, Y., Satyan, N., Rakuljic, G. & Yariv, A. Quantum control of phase fluctuations in semiconductor lasers. *Proc. Natl. Acad. Sci.* **115**, E7896–E7904, DOI: 10.1073/pnas.1806716115 (2018). https://www.pnas.org/content/115/34/E7896.full.pdf.

8. Harfouche, M. *et al.* Kicking the habit/semiconductor lasers without isolators. *Opt. Express* **28**, 36466–36475, DOI: 10.1364/OE.411816 (2020).

9. Zhang, Z. *et al.* High-speed coherent optical communication with isolator-free heterogeneous si/iii-v lasers. *J. Light. Technol.* **38**, 6584–6590, DOI: 10.1109/JLT.2020.3015738 (2020).

10. Henry, C. Theory of the linewidth of semiconductor lasers. *IEEE J. Quantum Electron.* **18**, 259–264, DOI: 10.1109/JQE.1982.1071522 (1982).

11. Hoefler, G. E. *et al.* Foundry development of system-on-chip inp-based photonic integrated circuits. *IEEE J. Sel. Top. Quantum Electron.* **25**, 1–17, DOI: 10.1109/JSTQE.2019.2906270 (2019).

12. Yariv, A. & Yeh, P. *Photonics - Optical Electronics in Modern Communications* (Oxford, 2007), 6th ed edn.

13. Yariv, A. *Quantum Electronics* (New York: Wiley, 1989), 3rd ed edn.

14. Coldren, L. A., Corzine, S. W. & Mashanovitch, M. L. *Diode Lasers and Photonic Integrated Circuits* (Wiley, 2012), 2nd ed edn.

15. Vahala, K. & Yariv, A. Semiclassical theory of noise in semiconductor lasers - Part I. *IEEE J. Quantum Electron.* **19**, 1096–1101, DOI: 10.1109/JQE.1983.1071986 (1983).

16. Vahala, K. & Yariv, A. Semiclassical theory of noise in semiconductor lasers - Part II. *IEEE J. Quantum Electron.* **19**, 1102–1109, DOI: 10.1109/JQE.1983.1071984 (1983).

17. Rideout, W. *et al.* Measurement of the carrier dependence of differential gain, refractive index, and linewidth enhancement factor in strained-layer quantum well lasers. *Appl. Phys. Lett.* **56**, 706–708, DOI: 10.1063/1.102688 (1990). http://dx.doi.org/10.1063/1.102688.

18. Ukhanov, A. A., Stintz, A., Eliseev, P. G. & Malloy, K. J. Comparison of the carrier induced refractive index, gain, and linewidth enhancement factor in quantum dot and quantum well lasers. *Appl. Phys. Lett.* **84**, 1058–1060, DOI: 10.1063/1.1647688 (2004). http://dx.doi.org/10.1063/1.1647688.

19. Petermann, K. *Laser Diode Modulation and Noise* (Springer Netherlands, Dordrecht, 1988).

20. Matsui, Y., Murai, H., Arahira, S., Kutsuzawa, S. & Ogawa, Y. 30-GHz bandwidth 1.55-μm strain-compensated InGaAlAs-InGaAsP MQW laser. *IEEE Photonics Technol. Lett.* **9**, 25–27, DOI: 10.1109/68.554159 (1997).

21. Kobayashi, W. *et al.* 50-Gb/s direct modulation of a 1.3-μm InGaAlAs-based DFB laser with a ridge waveguide structure. *IEEE J. Sel. Top. Quantum Electron.* **19**, 1500908–1500908, DOI: 10.1109/JSTQE.2013.2238509 (2013).

22. Wang, H. *et al.* Narrow-linewidth oxide-confined heterogeneously integrated si/iii–v semiconductor lasers. *IEEE Photonics Technol. Lett.* **29**, 2199–2202, DOI: 10.1109/LPT.2017.2771222 (2017).

23. Vahala, K., Chiu, L. C., Margalit, S. & Yariv, A. On the linewidth enhancement factor α in semiconductor injection lasers. *Appl. Phys. Lett.* **42**, 631–633, DOI: 10.1063/1.94054 (1983). http://dx.doi.org/10.1063/1.94054.

24. Zhao, B. *et al.* Direct measurement of linewidth enhancement factors in quantum well lasers of different quantum well barrier heights. *Appl. Phys. Lett.* **62**, 1591–1593, DOI: 10.1063/1.108647 (1993). http://dx.doi.org/10.1063/1.108647.

25. Komljenovic, T. *et al.* Widely tunable narrow-linewidth monolithically integrated external-cavity semiconductor lasers. *IEEE J. Sel. Top. Quantum Electron.* **21**, 214–222, DOI: 10.1109/JSTQE.2015.2422752 (2015).

26. Huang, D. *et al.* High-power sub-khz linewidth lasers fully integrated on silicon. *Optica* **6**, 745–752, DOI: 10.1364/OPTICA.6.000745 (2019).

27. Bimberg, D. *et al.* InGaAs-GaAs quantum-dot lasers. *IEEE J. Sel. Top. Quantum Electron.* **3**, 196–205, DOI: 10.1109/2944.605656 (1997).

28. Newell, T. C. *et al.* Gain and linewidth enhancement factor in InAs quantum-dot laser diodes. *IEEE Photonics Technol. Lett.* **11**, 1527–1529, DOI: 10.1109/68.806834 (1999).

29. Larson, M. C. *et al.* High performance widely-tunable SG-DBR lasers. In Gmachl, C. F. & Bour, D. P. (eds.) *Novel In-Plane Semiconductor Lasers II*, vol. 4995, 66 – 80, DOI: 10.1117/12.475792. International Society for Optics and Photonics (SPIE, 2003).

Acknowledgements

This work was supported by US Army Research Office (ARO) (W911NF-14-P-0020, W911NF-15-1-0584, W911NF-16-C-0026, W911NF-16-C-0105) and Defense Advanced Research Projects Agency (DARPA) (N66001-14-1-4062). The authors would like to thank the Kavli Nanoscience Institute (KNI) at Caltech for providing fabrication facilities for this work.

Author contributions

A.Y. conceived the project, directed it, and acquired funding. D.K. and M.H. designed the laser. D.K and H.W. performed the device fabrication. D.K., M.H., and H.W. conducted the measurements for the laser characteristics. D.K. and M.H. wrote the manuscript with inputs from all authors. C.S., Y.V., N.S. G.R. were instrumental in conceiving the design of the lasers and experimental setup.

Supplementary Files

This is a list of supplementary files associated with this preprint. Click to download.

- ModulationPaperSupplementary.pdf